The Sensitivity of Magnetic Anisotropy in the Solid State for Lanthanide Complexes with Small Crystal Field Splitting

Michele Vonci[a], *Kevin Mason*[b], *Emily R. Neil*[b], *Dmitry S. Yufit*[b], *Eric J. L. McInnes*[a], *David Parker*[b,*] *and Nicholas F. Chilton*[a,*]

[a]School of Chemistry and Photon Science Institute, The University of Manchester, Oxford Road, Manchester, M13 9PL, UK. [b]Department of Chemistry, Durham University, South Road, Durham, DH1 3LE, UK

Abstract

Knowledge of the crystal structure of a monometallic inorganic molecule is often sufficient to calculate its electronic structure and interpret its magnetic properties. Here we show that for a series of nine-coordinate lanthanide complexes based on the 1,4,7-tris[(6-carboxypyridin-2-yl)methyl]-1,4,7-triazacyclononane ligand, the electronic structure is hypersensitive to geometric structure and to the presence of non-coordinated lattice solvent, which renders the magnetic and spectroscopic properties very difficult to interpret. We explore possible explanations for the peculiar electron paramagnetic resonance (EPR) spectra and conclude that a number of entangled factors are at play across the samples, and hence that great care should be taken in the

interpretation of EPR spectra for systems with small magnetic anisotropy, even when the molecular structure is known.

Introduction

Complexes of trivalent lanthanides are employed in applications spanning paramagnetic probes in protein structure determination[1] to contrast agents in magnetic resonance imaging,[2] and have also been proposed in new technologies such as molecule-scale data storage.[3,4] To develop next-generation MRI contrast agents with enhanced sensitivity compared to traditional Gd-based agents, complexes of the late lanthanides ($4f^{8\text{-}13}$) have been proposed as PARASHIFT reagents where the dipolar pseudo-contact shift (δ_{pc}) is used to provide contrast.[5,6] This effect arises from the magnetic anisotropy of the Ln^{III} center and is commonly rationalized with the long-standing theory devised by Bleaney (Eq. 1; C_J is a constant for each Ln^{III} ion; β is the Bohr-magneton; k is the Boltzmann constant; B_2^0 and B_2^2 are the axial and rhombic second-rank crystal field parameters, respectively; r, θ, φ are the polar coordinates of the nucleus from the Ln^{III} ion; χ_{ax} and χ_{rh} are the axial and rhombic anisotropies of the magnetic susceptibility).[7,8]

$$\delta_{pc} = -\frac{C_J\beta^2}{60(kT)^2}\left[B_2^0\frac{3\cos^2\theta-1}{r^3}+B_2^2\frac{\sin^2\theta\cos2\varphi}{r^3}\right] = \frac{1}{12\pi r^3}\left[\chi_{ax}(3\cos^2\theta-1)+\frac{3}{2}\chi_{rh}\sin^2\theta\cos2\varphi\right] \quad (1)$$

Bleaney's treatment highlights the central role of the magnetic anisotropy, and by extension the local electronic structure, in determining magnitude and sign of δ_{pc}. Common implementations of Bleaney's theory assume that chemically analogous Ln complexes will possess the same crystal field parameterizations (*i.e.* B_2^0 and B_2^2 in Eqn. 1) and therefore that δ_{pc} for a series of

complexes is dictated solely by C_J (which is a constant for each Ln^{III} ion). However, this simplification has been shown to be grossly inadequate in some cases.[9,10]

In order to design better-performing PARASHIFT contrast agents, it is of paramount importance to investigate the origin of these discrepancies and establish a reliable relationship between molecular geometry, electronic structure/magnetic anisotropy, and δ_{pc}, in a similar way that the design of single-molecule magnets critically depend on the coordination enviroment.[3,11,12] We recently reported a theoretical and experimental study of paramagnetic NMR properties in solution of the C_3-symmetric nine-coordinated lanthanide series [LnL^1] (Ln = Eu, Tb, Dy, Ho, Er, Tm, and Yb; H_3L^1 = 1,4,7-tris[(6-carboxypyridin-2-yl)methyl]-1,4,7-triazacyclononane) (Figure 1).[9] Our work showed that the geometry of the [LnL^1] series results in a peculiar near-zero value for the second rank axial crystal field parameter (CFP) B_2^0. Under minimal perturbations of the first coordination sphere – such as those induced by the interactions with solvent molecules – small changes in the magnitude of B_2^0 can easily alter its sign, with dramatic effects on δ_{pc} and the luminescence spectra of the molecules. The take-home-message is that for certain families of molecules, despite apparent isostructurality in solution, the CFPs cannot be considered constant and they may not even possess a constant sign.

To overcome the most significant unknown in our solution studies, *viz* the lack of a known molecular structure, we decided to investigate the magnetic properties of the [LnL^1] series, as well as of two related series [LnL^2] (H_3L^2 = *P,P′,P″*-[(hexahydro-1*H*-1,4,7-triazacyclononane-1,4,7-triyl)tris(methylene-6,2-pyridinediyl)]tris[*P*-phenyl-), and [LnL^3][CF_3SO_3]$_3$ (L^3 = 2-Pyridinecarboxamide, 6,6',6"-[(hexahydro-1*H*-1,4,7-triazacyclononane-1,4,7-triyl)tris(methylene)]tris[N-[1-phenylethyl]-) (Ln = Tb, Dy, Ho, Er, Tm, and Yb) (Figure 1), in

the crystalline phase where the molecular structures are measurable. The three series of compounds, [LnL^1], [LnL^2], and [LnL^3][CF_3SO_3]$_3$, have therefore been investigated by single crystal X-ray diffraction (XRD), and by magnetometry and multifrequency electron paramagnetic resonance (EPR) spectroscopy in the solid state.

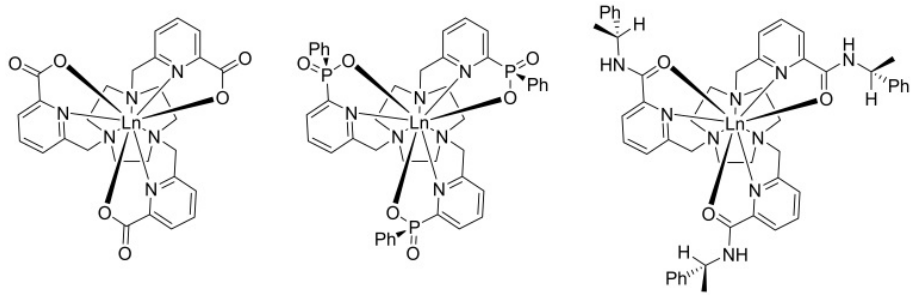

Figure 1. Schematic representation of the [LnL^1], [LnL^2], and [LnL^3]$^{3+}$ complexes.

Experimental

We have collected new single crystal XRD data for compounds [TmL^1], [TbL^3][CF_3SO_3]$_3$, [DyL^3][CF_3SO_3]$_3$, [HoL^3][CF_3SO_3]$_3$, [ErL^3][CF_3SO_3]$_3$, [TmL^3][CF_3SO_3]$_3$ and [YbL^3][CF_3SO_3]$_3$ here, while the structures for [TbL^1], [YbL^1], [HoL^2], [TmL^2], and [YbL^2] have been reported earlier.[13,14,15,16,17] The structures of [TbL^2], [DyL^1], [DyL^2], [HoL^1], [ErL^1], and [ErL^2] are as-yet undetermined due to the lack of suitable single crystals. Single crystal XRD data was collected using Mo-K_α radiation (λ = 0.71073 Å) on a Bruker D8Venture (Photon100 CMOS detector, IμS-microsource, focusing mirrors) diffractometer equipped with an Oxford Cryosystems Cryostream open-flow nitrogen cryostat. The Helix (Oxford Cryosystems) open-flow helium cryostat has been used for data collection at 30 K for the compound [YbL^3][CF_3SO_3]$_3$. Single crystals were placed under a stream of cold nitrogen at 250 K and then cooled to 150.0(2) K at 120 K h^{-1} to prevent deterioration of crystal quality during flash-cooling. Structures were solved by direct methods and refined by full-matrix least squares on F^2 for all data using Olex2[18] and SHELXTL[19,20] software. All non-disordered non-hydrogen atoms were refined anisotropically, while the hydrogen atoms were placed in the calculated positions and refined in riding mode. Disordered atoms in the anions were refined isotropically with fixed SOF = 0.5, while the methyl groups of methanol solvent molecules which are disordered over three positions were refined with fixed SOF = 0.167. One of the water molecules in the structure of [TmL^1] is disordered over two positions and refined with fixed SOFs 0.7 and 0.3. Crystal data and parameters of refinement are given in the SI (Table S1). Crystallographic data for the structures have been deposited with the Cambridge Crystallographic Data Centre as supplementary publication CCDC-1879271, 1879268, 1879264, 1879265, 1879272, 1879266, 1879267, 1879270.

CASSCF-SO calculations were performed with MOLCAS 8.0[21] using the CASSCF/RASSI/SINGLE_ANISO approach,[22] employing structures as determined by XRD with no optimization. Where the crystal structure was not available, the structure of the complex containing the nearest neighbor lanthanide ion was used (Table S2).[23] Only molecules bound to the Ln ion were included in the calculation, thus non-coordinating solvent and counter ions were omitted. In all calculations the Ln atoms were treated with the ANO-RCC-VTZP basis, the N and O donor atoms with the ANO-RCC-VDZP basis, while all other atoms were treated with the ANO-RCC-VDZ basis.[24] In order to save disk space the two electron integrals were decomposed using the Cholesky decomposition with a threshold of 10^{-8}. The electronic configurations of Tb^{III} ($4f^{8}$), Dy^{III} ($4f^{9}$), Ho^{III} ($4f^{10}$), Er^{III} ($4f^{11}$), Tm^{III} ($4f^{12}$), and Yb^{III} ($4f^{13}$) were modelled with a complete active space of 8, 9, 10, 11, 12, and 13 electrons, respectively, in the 7 4*f* orbitals. The spin multiplets that were included in the RASSCF orbital optimization of the spin-only wave functions as well as the number of states mixed by spin-orbit coupling by RASSI are reported in Table S3. The SINGLE_ANISO module was used to compute the magnetic properties of the complexes and to obtain the CFPs by projecting the lowest lying CASSCF-SO wave functions onto a $(2J + 1)$-dimensional pseudo-spin basis.[25] These CFPs were used with the software PHI[26] in order to simulate the in-field magnetic susceptibility temperature dependence and CW EPR spectra.

Magnetic measurements were performed with a Quantum Design SQUID magnetometer on unrestricted polycrystalline samples. Due to the compensating effects on the crystal field by the three sets of donor atoms,[9] the magnetic anisotropy is rather small in these compounds, embodied by the near-zero value of B_2^0. Thus we do not expect that magnetic torque is strong enough to cause alignment of the crystallites by the applied field, and so the unrestrained

samples are not expected to give spurious results. The magnetic susceptibility was measured between 2 – 300 K under an applied field of 10 kOe, while the isothermal field dependence of the magnetization was measured between 0 – 70 kOe at 2 and 4 K. EPR spectra were collected at X- and Q-band with a Bruker EMX300 spectrometer at 5 K with crushed crystalline samples.

Results

Molecular structure

The three series of complexes show a similar coordination environment (Figure 2). Each one features a 9-coordinate Ln^{III} ion with three sets of donor atoms: three nitrogen atoms from the macrocyclic ring (N_{tacn}), three nitrogen atoms from the pyridyls (N_{py}) and three oxygen atoms from the functional group of the pyridyls (carboxylate for L^1, phenylphosphinate for L^2, phenyl amide for L^3) For some of the complexes in the [LnL^1] and [LnL^2] series – [TbL^2], [DyL^1], [DyL^2], [HoL^1], [ErL^1], and [ErL^2] – it was impossible to grow single crystals suitable for XRD. Due to the scarcity of product we have been unable to collect PXRD traces for these complexes. However, in all cases where XRD data is unavailable, we were able to collect data for Ln analogues having both larger and smaller ionic radii showing that the complexes on either side are isomorphous; this strongly suggests that all complexes in each of the [LnL^1] and [LnL^2] series are indeed isomorphous.

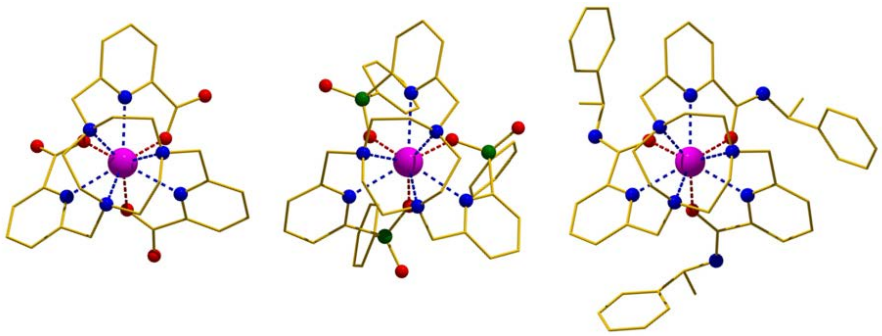

Figure 2. Structures of the neutral complexes [TmL^1] (left), [TmL^2] (center), and the cation, S-Δ-(λλλ)-[TmL^3]$^{3+}$ (right). Ln = magenta, N = blue, O = red, P = green, C = yellow, H-atoms and solvent molecules omitted for clarity.

The carboxylate complexes [LnL^1] crystallize from aqueous solution in the monoclinic space group Pn, with three waters of crystallization. The XRD structures of the Eu, Nd, Gd, Tb , Yb and Lu complexes have been reported earlier,[13,14,27] and here we report the Tm structure. Despite the lack of a crystallographic C_3 axis, these molecules have pseudo 3-fold symmetry (where we define the pseudo-C_3 axis as the vector joining the Ln ion and the centroid of the O-donor atoms), with only small variations found in bond lengths of chemically equivalent donor atoms (Table 1).

Table 1. Selected mean distances of the ligand donor atoms to the Ln^{III} ion in [LnL^1][a]

Ln^{III}	Eu	Gd	Tm	Yb	Lu
Ln-O / Å	2.39(2)	2.38(2)	2.32(2)	2.31(2)	2.31(2)
Ln-N_{ring} / Å	2.67(2)	2.67(2)	2.61(2)	2.61(2)	2.61(2)
Ln-N_{py} / Å	2.56(1)	2.55(1)	2.49(1)	2.483(4)	2.49(1)
θ (Ln-O) / °	51.4(4)	51.3(3)	50.1(3)	50.0(4)	50.0(2)
θ (Ln-N_{ring}) / °	140.9(4)	140.7(3)	140.3(2)	140.2(2)	140.1(4)
θ (Ln-N_{py}) / °	89(1)	89(1)	88.5(8)	88.5(9)	88.6(7)

[a] All metal ligand distances are crystallographically independent, and the mean value is given with the standard deviation in parentheses. For the Eu, Gd and Lu structures see CCDC 206376-206378; for Yb see CCDC 1850294.

The phenylphosphinate series [LnL^2] crystallize from water/methanol solutions in the monoclinic space group $P2_1/n$. The Ce, Nd, Sm, Eu, Ho, Tm, and Yb XRD structures have previously been reported and are isomorphous.[15,16] From previous studies these structures contain an unknown number of highly disordered H_2O and/or MeOH molecules and the XRD structures were refined

using a solvent mask.[15,16] However, to treat the magnetic data meaningfully the molecular weight needs to be known with sufficient accuracy. Combining the electron content of the XRD solvent mask, thermogravimetric analysis, and elemental analysis, we determined that in [HoL^2] there are 10 disordered H_2O molecules and one disordered molecule of methanol per formula unit (Figure S1 and Tables S4-S5); we assume this is a reasonable approximation for all [LnL^2] complexes. As for the [LnL^1] series, the [LnL^2] series are close to three-fold symmetric despite the absence of a crystallographic C_3 axis (Table 2); again, the pseudo-C_3 axis is defined as the vector joining the Ln ion and the centroid of the O-donor atoms.

Table 2. Selected mean distances of the ligand donor atoms to the Ln^{III} ion in $[LnL^2]$[a]

Ln^{III}	Ln^{III}	Eu	Ho	Tm	Yb
Ln-O / Å	Ln-O / Å	2.332(8)	2.289(6)	2.260(4)	2.252(6)
Ln-N_{ring} / Å	Ln-Nring / Å	2.68(2)	2.65(2)	2.63(3)	2.63(2)
Ln-N_{py} / Å	Ln-Npy / Å	2.66(1)	2.63(1)	2.62(2)	2.62(2)
θ (Ln-O) / °	θ (Ln-O) / °	52.1(8)	51.4(9)	51(1)	51(1)
θ (Ln-N_{ring}) / °	θ (Ln-Nring) / °	141.0(8)	140.7(7)	140(1)	140.5(9)
θ (Ln-N_{py}) / °	θ (Ln-Npy) / °	90.0(9)	90.0(8)	90(1)	90(1)

[a] All metal ligand distances are crystallographically independent, and the mean value is given with the standard deviation in parentheses; CCDC 836097, 836098, 836101 and 836102.

Crystals of $[LnL^3][CF_3SO_3]_3$ grow readily from aqueous methanol (1:1). The complexes crystallize in the trigonal space group R3, and form an isomorphous series (Table 3). The Eu and Yb structures were reported previously[17] and here we report the Tb, Dy, Ho, Er, Tm structures: in each case, the anions were slightly disordered and a MeOH solvent molecule with a disordered methyl group was also present. In this family, a C_3 crystallographic axis passes through the metal ion, the centroid of the macrocycle, and the O-H bond of the non-coordinated methanol molecule.

Table 3. Selected mean distances of the ligand donor atoms to the Ln^{III} ion in $[LnL^3][CF_3SO_3]_3$[a]

Ln^{III}	Eu[b]	Gd	Tb	Dy	Ho	Er	Tm	Yb[a]
Ln-O / Å	2.405(3)	2.393(2)	2.384(2)	2.372(2)	2.364(2)	2.353(2)	2.344(2)	2.344(4)
$Ln\text{-}N_{ring}$ / Å	2.628(3)	2.619(2)	2.607(2)	2.598(2)	2.589(3)	2.582(2)	2.575(2)	2.572(4)
$Ln\text{-}N_{py}$ / Å	2.567(3)	2.556(2)	2.544(2)	2.533(2)	2.524(2)	2.515(2)	2.506(2)	2.487(4)
θ (Ln-O) / °	50.80(6)	50.54(5)	50.29(5)	50.10(5)	49.90(5)	49.72(6)	49.46(6)	49.09(8)
θ ($Ln\text{-}N_{ring}$) / °	140.13(8)	140.00(5)	140.00(5)	139.91(5)	139.72(5)	139.74(5)	139.70(5)	139.5(1)
θ ($Ln\text{-}N_{py}$) / °	88.12(8)	87.86(5)	87.76(5)	87.65(5)	87.54(5)	87.59(5)	87.49(5)	87.3(1)

[a] All metal ligand distances are crystallographically identical, and the standard deviation from refinement is given in parentheses. [b] Data for the Eu and Yb complexes are from CCDC 965909–965911.

The comparison of the $\{LnO_3N_6\}$ coordination environments across the three series of compounds is complicated by the lack of rigorous three-fold symmetry in $[LnL^1]$ and $[LnL^2]$, in contrast to $[LnL^3]^{3+}$. In the discussion that follows, the bond distances and angles for $[LnL^1]$ and $[LnL^2]$ are averaged values having a relatively large variability compared to the uncertainties in $[LnL^3]^{3+}$ (Tables 1-3). For all three series, the polar angles (θ) with respect to the (pseudo-)C_3 axis for the three sets of donor atoms decrease with the radius of the lanthanide, indicating that smaller Ln ions tend to move towards the macrocyclic cavity where they are better accommodated. The Ln-O and $Ln\text{-}N_{py}$ distances are similar for $[LnL^1]$ and $[LnL^3]^{3+}$, with $[LnL^2]$ having smaller Ln-O distances and larger $Ln\text{-}N_{py}$ distances: such behavior is unsurprising, given the similarity in the pyridyl-carbonyl donors for L^1 and L^3 *cf.* the pyridyl-phosphinate of L^2. The $Ln\text{-}N_{ring}$ distances are similar in $[LnL^1]$ and $[LnL^2]$ while those for $[LnL^3]^{3+}$ are smaller: however, the variations in $Ln\text{-}N_{ring}$ across $[LnL^{1\text{-}3}]$ are significantly smaller than those in L-O/N_{py}.

Magnetic properties and electronic structure

The room temperature χT value (where χ is the molar magnetic susceptibility) of all [LnL^{1-3}] complexes are close to the expected Curie limit for free Ln^{III} ions based on the $^{2S+1}L_J$ Russel Saunders ground terms (Table S6). In each case χT decreases with decreasing temperature due to Boltzmann population changes within the CF-split ground total angular momentum *J* manifold (Figure 3). Low temperature magnetization (*M*) *vs.* applied magnetic field (*H*) data at 2 and 4 K (Figures S2-S4) show different profiles for different ions: the Kramers ions (Dy^{III}, Er^{III}, and Yb^{III}) always show clearly separated traces for the two temperatures, while the non-Kramers ions (Tb^{III}, Ho^{III}, and Tm^{III}) always show nearly overlaid traces – the latter is indicative of singlet ground states for these non-Kramers species. The magnetization data also show that the ground state for a given Ln^{III} ion is strongly affected by whether it is coordinated to L^1, L^2, or L^3. The data for [LnL^1] and [LnL^3][CF_3SO_3]$_3$ – with similar pyridyl-carbonyl donors (and hence similar structures) – are generally similar to one another, while those for [LnL^2] – with pyridyl-phosphinate donors – generally stand out (Figure 4) .

To model the electronic structure and magnetic properties of these complexes, we have performed CASSCF-SO calculations using the known XRD geometries (Tables S7 – S15). As the structures of [TbL^2], [DyL^1], [DyL^2], [HoL^1], [ErL^1], and [ErL^2] are unknown, we have used the nearest neighbor structure (Table S2); given the structural sensitivity of these samples[9] this is not *a priori* a good approximation, but we show below that even knowledge of the crystal structure does not appear satisfactory to explain the behavior of these compounds in the solid state from CASSCF-SO *ab initio* methods. The CASSCF-SO-calculated χT traces (Figure 3) are

in good agreement with the experimental data at high temperatures, but deviate at lower temperatures. The low temperature discrepancies of CASSCF-SO-calculated χT traces are also highlighted by generally poor agreement between calculated and experimental $M(H)$ data at 2 K (Figure 4). Although some specific examples give excellent agreement for $M(H)$, *viz*. [DyL^1], [TbL^1], [ErL^2], [TmL^3][CF_3SO_3]$_3$ and [YbL^1], there is no obvious pattern. We note that despite having the crystal structure for 12 of these species, the calculated magnetic data obtained from these structures do not always give good agreement at low temperatures, and also that we observe excellent agreement for some examples where we have used surrogate structures (*e.g.* for [DyL^1] and [ErL^2]). Hence, our single-point CASSCF-SO calculations do not consistently capture the ground state wavefunctions of these compounds.

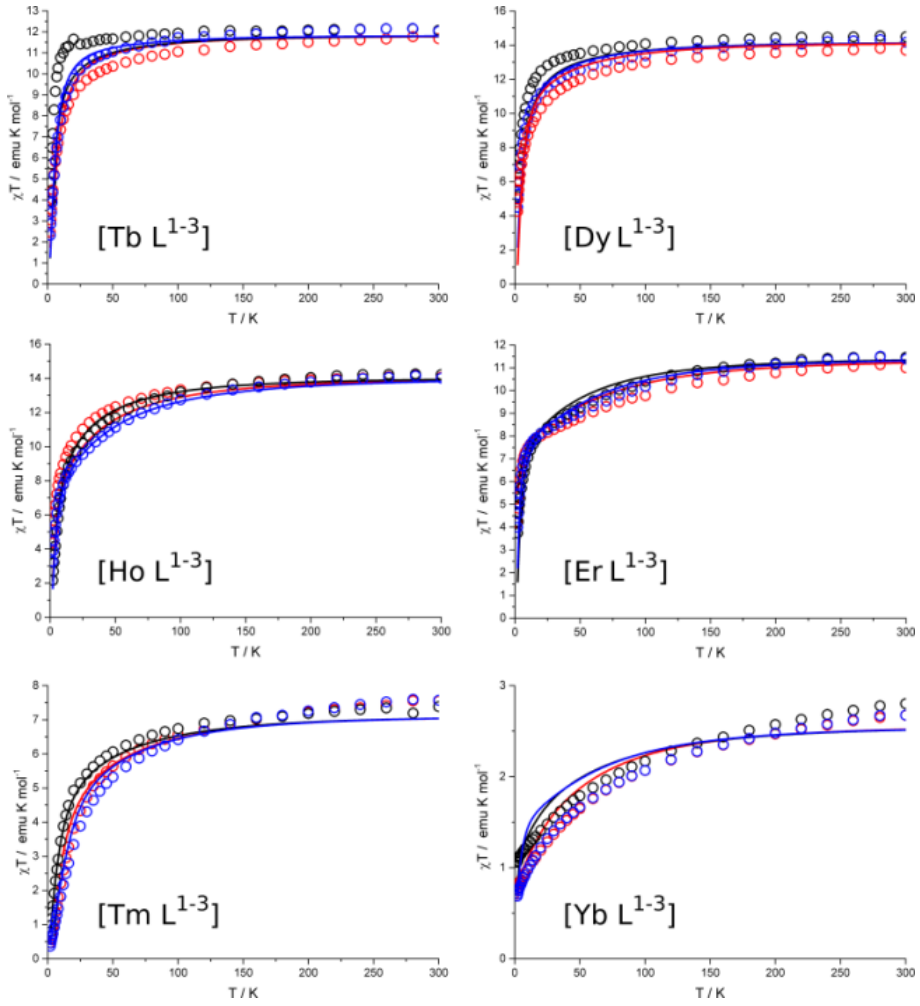

Figure 3. Experimental (circles) and CASSCF-SO *ab initio* (solid lines) temperature dependence of χT for [LnL^1] (red), [LnL^2] (black), and [LnL^3]$^{3+}$ (blue) in the 2 – 300 K range (inset 0-5 K).

To probe directly the character of the ground states, we have employed multi-frequency EPR spectroscopy of the nine complexes containing Kramers ions: [DyL$^{1-3}$], [ErL$^{1-3}$] and [YbL$^{1-3}$] (*M*(*H*) data shows that the non-Kramers ions have singlet ground states and will thus be EPR silent). Each one gives rich and very anisotropic spectra at X- and Q-band frequencies and 5 K

(Figure 5); despite the “ugly” nature of some of these spectra, duplicate measurements on fresh sample batches gave identical results. Usually, liquid helium temperature EPR spectra of Kramers Ln^{III} ions are ably interpreted with the effective $S = 1/2$ model, as the lowest Kramers doublet is well-isolated at such temperatures. With the exceptions of $[YbL^2]$ and $[YbL^3][CF_3SO_3]_3$, the present EPR spectra can be modelled in this manner (with varying degrees of success) giving rhombic (L^1 and L^2) or axially symmetric (L^3) effective *g*-values (Figure 5, Table 4, Table S16). However, these models are complicated by requiring highly anisotropic and large linewidths. The fitted spectra show the best agreement for $[ErL^2]$ and $[YbL^1]$. We note that hyperfine coupling to spin-active Ln^{III} nuclei is only clearly observable for $[YbL^{1\text{-}3}]$.

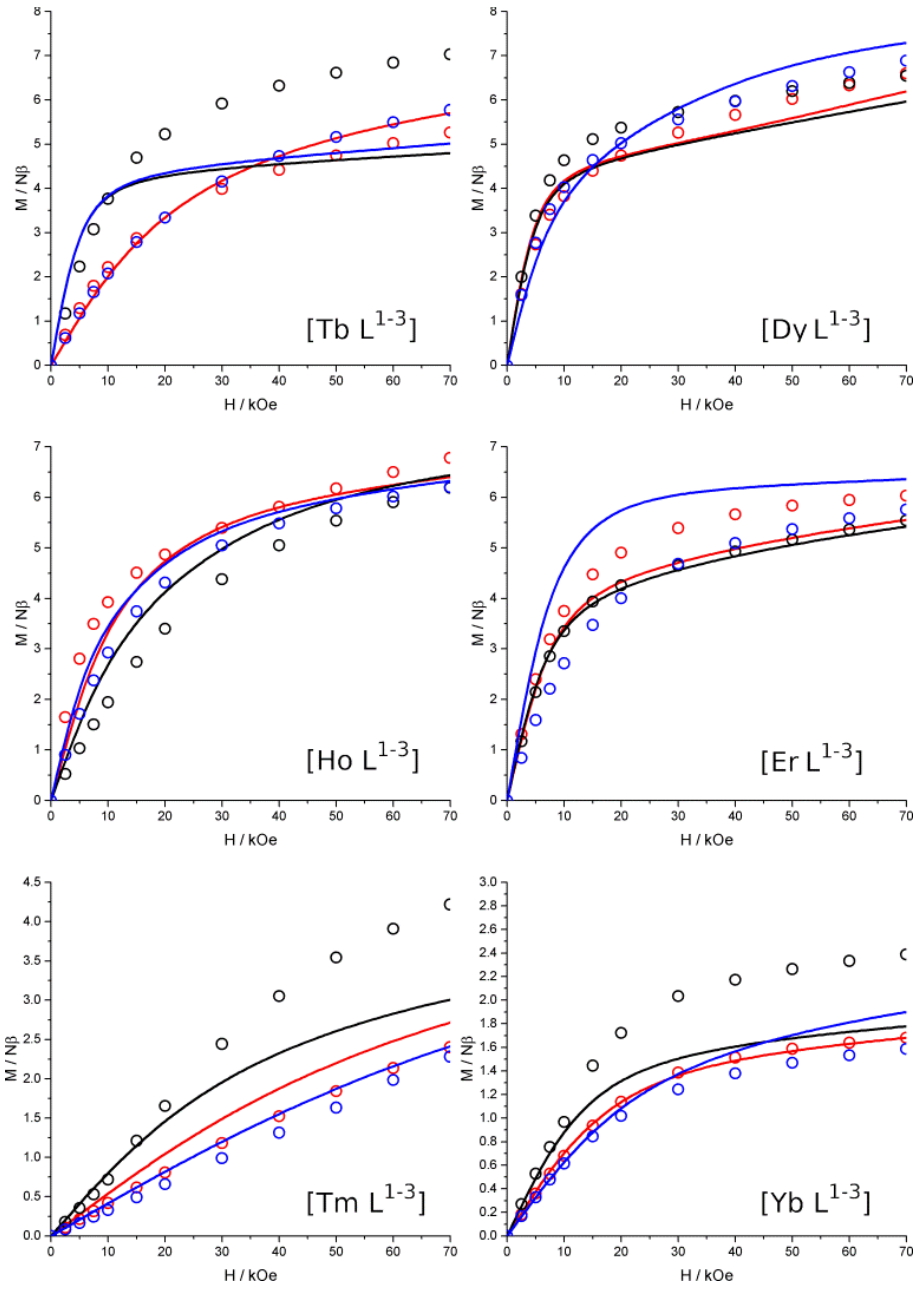

Figure 4. Experimental (circles) and CASSCF-SO *ab initio* (solid lines) magnetic field dependence of *M* in the 0 – 70 kOe range, and at 2 K, for [LnL^1] (red), [LnL^2] (black), and [LnL^3]$^{3+}$ (blue).

Only in the cases of [DyL^1], [ErL^2], and [YbL^1] are the effective *g*-values remotely similar to those calculated by CASSCF-SO for the ground Kramers doublet (Table S16): note these are the examples that also give good agreement to *M*(*H*), and that the calculations for [DyL^1] and [ErL^2] were performed on surrogate crystal structures. Indeed, the experimental *g*-values for [DyL^2], [DyL^3], and [ErL^1] are closer to those calculated for the first excited doublets state (Table S16). Notably, use of an *S* = 1/2 model cannot reproduce the complexity of the spectra observed for [YbL^2] and [YbL^3][CF_3SO_3]$_3$.

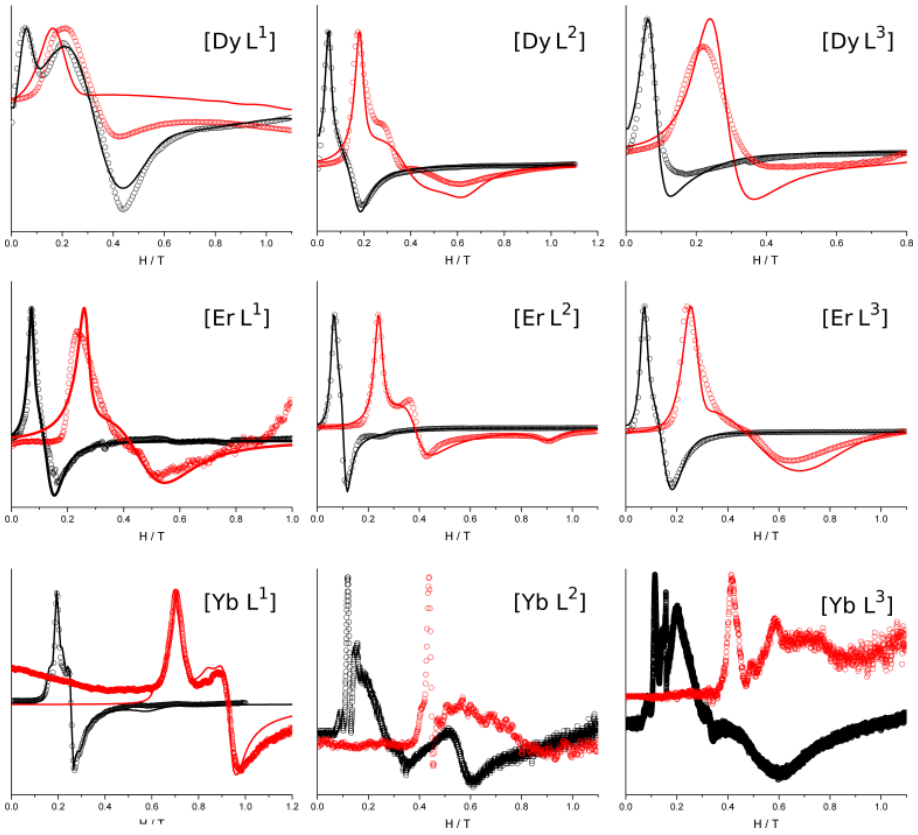

Figure 5. Experimental (open circles) and S =1/2 model simulations (solid line) at X (black) and Q (red) – band CW EPR spectra at 5K for [LnL$^{1-3}$] (Ln = Dy, Er, Yb).

Discussion

Overall, our CASSCF-SO calculations for [DyL^1], [ErL^2] and [YbL^1] are in good agreement with magnetic and EPR data. However, the experimental data for the remaining [LnL^{1-3}] suggest that CASSCF-SO calculations performed using known crystal structures still seem to be inadequate for determination of the electronic structure. It is interesting that this conclusion is not simply due to the substitution of crystal structures – for example, although we have the structures of [TbL^2], [TmL^2] and [YbL^2], our calculations are in poor agreement at low temperatures for these compounds, and yet are in good agreement for [DyL^1] and [ErL^2] which have been performed on surrogate structures. Furthermore, the EPR spectra for most samples have very broad and anisotropic lines, and those for [YbL^2] and [YbL^3][CF_3SO_3]$_3$ defy interpretation with a simple S = 1/2 model. For these latter Yb^{III} complexes, a S = 1/2 model with inclusion of the hyperfine coupling can explain some of the sharpest features at low field (*e.g.* for [YbL^1], Table 4), however this does not account for the broad features at higher fields. We note that due to very broad lines in some cases (*i.e.* [DyL^3][CF_3SO_3]$_3$) that there is some uncertainty in the reported g-values.

Therefore, we have investigated four potential causes of these broad spectra, by examining their impact on the electronic structures and magnetic properties of the [LnL^{1-3}] series. These are: (i) the CASSCF-SO-calculated value of B_2^0 is inaccurate; (ii) there is a distribution of molecular structures in the solid state; (iii) there is a temperature dependence of the crystal structure; (iv) disordered solvent leads to varying local environments. We focus on [YbL^3][CF_3SO_3]$_3$ in the main text, where the crystal structure is known, yet its powder EPR spectra cannot be modelled as S = 1/2, and the data for the other samples can be found in the supporting information. As [YbL^3][CF_3SO_3]$_3$ grows the nicest crystals of all [LnL^{1-3}], we attempted to collect a single crystal

EPR spectrum to shed light on these models, but we were unable to obtain any spectra from a number of crystals. We note that another contribution to the broad spectral features could be from dipolar magnetic interactions; these effects could be probed by dilution experiments in either solution or solid phase, however in the present case this would lead to more structural uncertainty and thus further complicate our analysis. Hence, we have performed all measurements on pure crystalline materials.

Table 4. Parameters derived from fitting EPR spectra for [LnL$^{1-3}$] using S = 1/2 models. The hyperfine parameters are fixed based on established relationships to the g-values.[34]

Compound	Experiment								CASSCF-SO		
	g_x	g_y	g_z	X-band LW (x, y, z; GHz)	Q-band LW (x, y, z; GHz)	A_x (cm^{-1})	A_y (cm^{-1})	A_z (cm^{-1})	g_x	g_y	g_z
[DyL^1]	0.0	2.1	14.1	(2.05, 6.18, 11.9)	(0.57, 73.2, 19.0)	-	-	-	0.04	1.58	17.10
[DyL^2]	3.9	6.7	13.2	(4.2, 20.0, 4.8)	(11.0, 24.0, 7.50)	-	-	-	0.10	1.09	16.85
[DyL^3]	9.3	9.3	3.3	(9.8, 9.8, 9.8)	(19.0, 19.0, 19.0)	-	-	-	0.03	0.11	11.60
[ErL^1]	5.0	5.0	9.1	(6.9, 6.9, 3.0)	(22.7, 22.7, 5.6)	-	-	-	2.60	6.87	10.18
[ErL^2]	2.7	6.3	10.1	(3.4, 3.2, 3.1)	(2.9, 6.5, 4.1)	-	-	-	2.14	6.49	10.74
[ErL^3]	4.3	4.3	9.0	(6.9, 6.9, 3.6)	(25.0, 25.0, 6.0)	-	-	-	8.72	8.18	3.02
[YbL^1]	1.15	2.60	3.45	(2.0, 0.5, 0.5)	(1.4, 1.4, 1.4)	^{171}Yb 1.28E-02 ^{173}Yb 3.56E-03	3.41E-02 9.73E-03	4.54E-02 1.30E-02	0.00	2.26	4.55
[YbL^2]	-	-	-	-	-	-	-	-	0.17	1.06	5.83
[YbL^3]	-	-	-	-	-	-	-	-	2.77	2.77	1.41

(i) Variation of electronic structure with B_2^0

We have shown previously that B_2^0 is near zero for [LnL^1] and that it is very sensitive to small structural distortions.[9] This implies that our CASSCF-SO-calculated electronic structures (and thus values of B_2^0) may be subject to significant error bars. The most significant structural parameter is the polar angle of the O-donors, which is readily altered by torsions of the pyridyl groups, and that B_2^0 (CF quantised along pseudo-C_3 axis) is the most sensitive CFP to this distortion.[9] We previously determined the variation of B_2^0 for a ±5° range of this torsion angle (around the DFT-optimised structures of [LnL^1], see Table S17 for ranges),[9] and thus we have calculated the electronic structure for [LnL$^{1\text{-}3}$] (Ln = Dy, Er, Yb) by varying B_2^0 in these pre-determined ranges. We start with the full set of 27 CFPs calculated by CASSCF-SO based on the crystal structure (or surrogate), and then systematically vary B_2^0 across the range described above (Figure 6). The limit of this approach is that we neglect the effect of inaccuracies in the other CFPs. However, given the dominant effect of B_2^0 on the magnetic anisotropy found previously for [LnL^1],[9] we suspect this is a fair approximation.

The electronic structures are, unsurprisingly, extremely sensitive to variations of B_2^0 such that the ground doublet can change its nature (*e.g.* from easy axis to easy plane) and that there is often a thermally accessible first excited doublet, even at 5 K, which would render the effective S = 1/2 EPR model invalid. Thus for each choice of B_2^0 in Figure 6, we have calculated EPR spectra at X- and Q-band using the full J manifold, incorporating the effect of all transitions between all CF states (Figure 7 and Figures S5-S22). Considering the exemplar case of [YbL^3][CF_3SO_3]$_3$, all individual values of B_2^0 give simple S = 1/2 spectral simulations at 5 K, although they change as

a function of B_2^0. It is interesting to note that the best agreement with the sharpest experimental features in the spectra of $[YbL^3][CF_3SO_3]_3$ is achieved for B_2^0 = -78 cm^{-1} (Figure 7c), which is quite close to the value of B_2^0 (-52 cm^{-1}) obtained by CASSCF-SO calculations on the XRD structure. Nonetheless, the broad features that we observe at X- (0.2 – 0.4 T) and Q-band (0.5 – 0.8 T) are completely unaccounted for in these simulations. The simulated temperature dependence for $[YbL^3][CF_3SO_3]_3$ in the 4 – 10 K range (Figures S21-S22) suggest that there are no contributions from excited doublets; such behaviour does not hold for some of the other complexes, notably $[DyL^{1\text{-}3}]$ and $[ErL^{1\text{-}3}]$ (Figures S5-S16). Therefore, for some compounds it is possible that depending on the actual value of B_2^0, a minimal experimental error in the real sample temperature could contribute to some of the observed discrepancies and/or the irregularly broad linewidths.

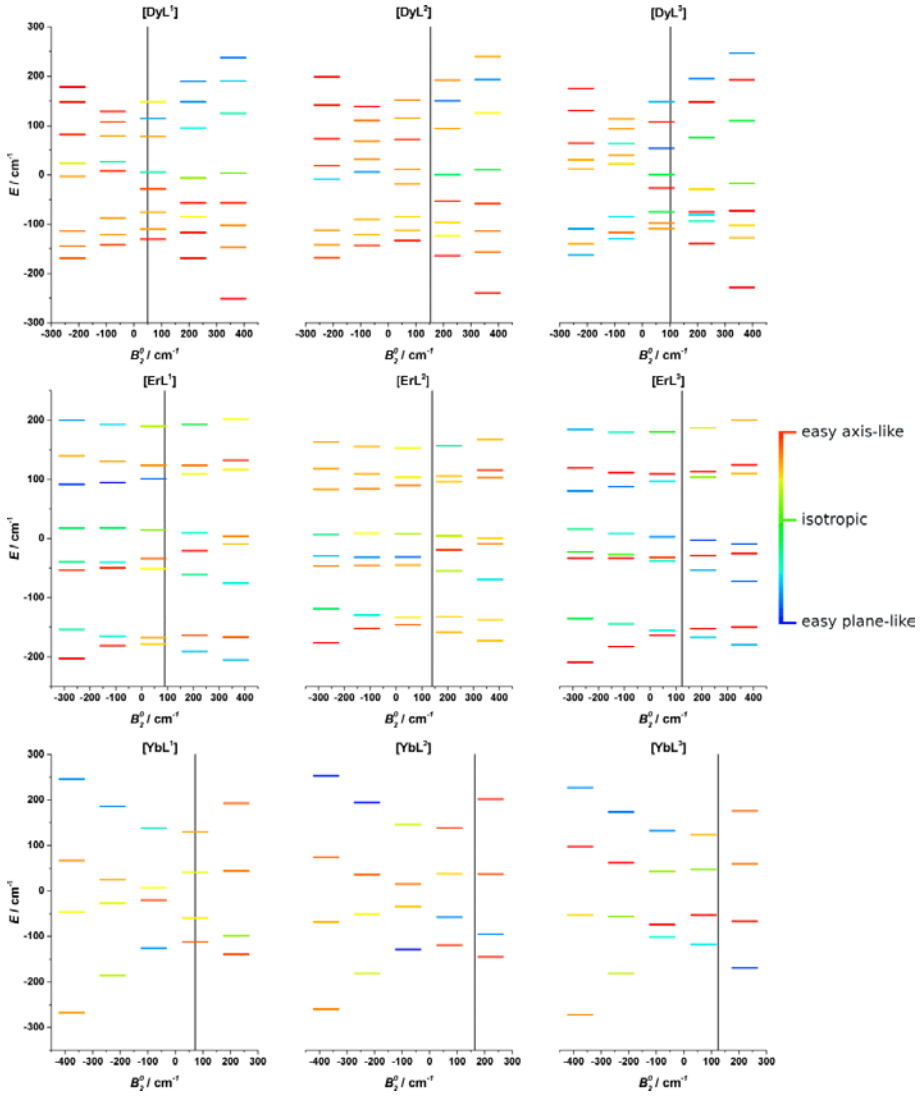

Figure 6. Energies of the states of the ground state *J* multiplets for [DyL$^{1\text{-}3}$], [ErL$^{1\text{-}3}$], and [YbL$^{1\text{-}3}$] as a function of B_2^0. The colour indicates the degree of axiality (towards easy-axis or easy-plane) in the anisotropy of the principal *g*-values for each Kramers doublet. Energies are referenced to the barycentre for each parameter set. Vertical lines correspond to the B_2^0 value obtained from CASSCF-SO calculations based on XRD data.

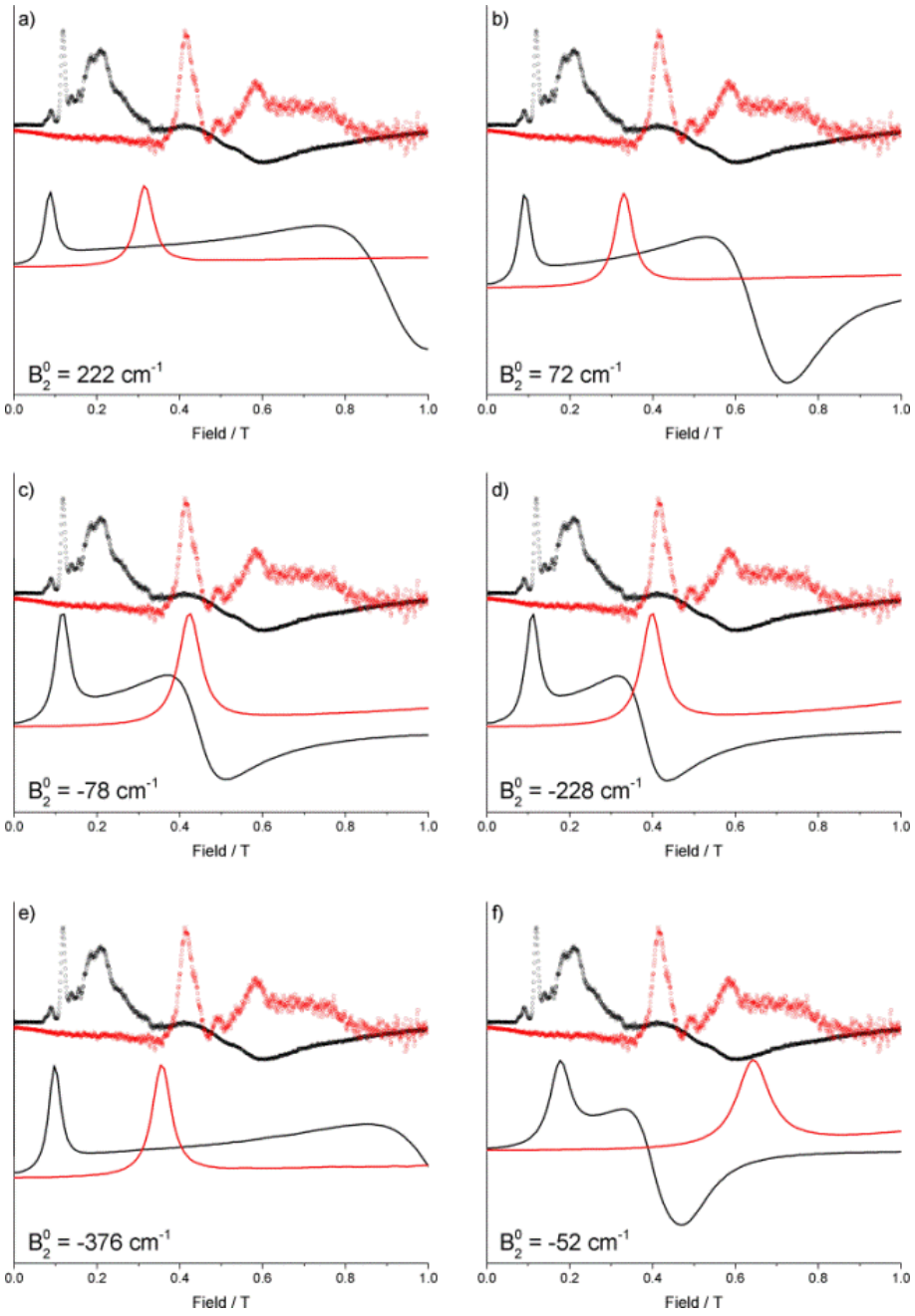

Figure 7. Experimental (open circles) and CASSCF-SO calculated (solid lines) CW X- (black) and Q-band (red) spectra at 5 K for [YbL^3][CF_3SO_3]$_3$, with different values of B_2^0. Panels a)-e) correspond the range of B_2^0 from solution studies, while panel f) is the result of CASSCF-SO on the XRD structure.

(ii) Distribution of structures

The calculated EPR spectra for [LnL$^{1\text{-}3}$] as a function of B_2^0 clearly demonstrate changes to the magnetic anisotropy of the ground states. Hence, if there were a distribution of structural parameters associated with crystallographic disorder and/or the presence of amorphous fractions in the samples (*e.g.* arising from grinding), this could yield a distribution of CFPs with a non-negligible and non-trivial effect on the EPR spectra. To investigate this effect, we consider a simple Gaussian distribution of B_2^0 where the standard deviation σ is related to the degree of structural variation in the sample. The observable EPR spectrum is then the Gaussian-weighted integral of the individual spectra comprising the distribution, each of which is assumed to have an isotropic linewidth. This simple model has the advantage of parameterizing structural variations with only two parameters. We have calculated powder EPR spectra and magnetic data with this approach, where the average value of B_2^0 is obtained from CASSCF-SO on the crystal structure (or surrogate), and $\sigma(B_2^0)$ is set as 25% of the range of B_2^0 associated with the ±5° pyridyl torsion studied above. For [YbL^3][CF_3SO_3]$_3$ the EPR spectra differ substantially between the single-point and Gaussian-distribution models (Figure 8; similar results observed for the other Kramers ions, Figures S23-S30); simulations obtained with a Gaussian distribution of B_2^0 qualitatively reproduce the numerous and broad features observed at X-band (0.2 – 0.4 T) and Q-band (0.5 – 0.8 T) for [YbL^3][CF_3SO_3]$_3$ (Figure 8).

This approach is particularly successful for explaining the spectra of [DyL^1] (Figure S23), giving the two broad shoulders in the X-band trace that cannot be accounted for with a S = 1/2 model. For the remaining [LnL$^{1\text{-}3}$], the Gaussian distribution model does not improve the simulated spectra. This is either because the model just broadens the lines without substantially altering the

spectrum (*e.g.* for [ErL^2], Figure S27), or perhaps because an inaccurate central value of B_2^0 from CASSCF-SO has placed the distribution in the wrong place (*e.g.* for [DyL^2], Figure S24). We note that this approach for modelling disorder is fundamentally distinct from commonplace "strain" models in EPR. "Strain" models assess the sensitivity of electronic states to changes in a spin Hamiltonian parameter and augment the linewidth of the transition.[28] Here, we directly account for a distribution of electronic structures: in cases where changes in B_2^0 lead to a change in the nature of the ground doublet, our model will show an effect on the EPR spectrum that cannot be reproduced by a "strain" model.

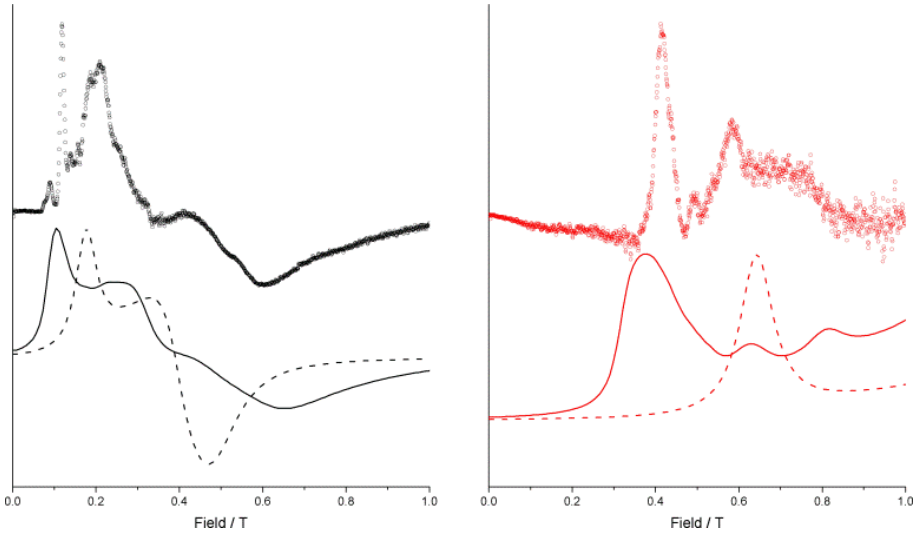

Figure 8. EPR simulations for [YbL^3][CF_3SO_3]$_3$. Experimental data (open circles), simulated EPR spectra with a single B_2^0 value (dashed line) and simulated EPR spectra with a Gaussian distribution of B_2^0 (solid line), at X-band (left) and Q-band (right). The Gaussian integral to account for the distribution of B_2^0 was approximated with 100 points across $B_2^0 \pm 4\sigma$, where B_2^0 = -52 cm^{-1} σ = 150 cm^{-1}.

(iii) Temperature dependent crystal structure

Another potential cause of the discrepancies could be thermal evolution of crystal structures. Our calculations are based on structures collected at 120-150 K while experiments are performed down to 2 K. To explore this possibility, we have collected an additional data set for the sample with the best crystals, $[YbL^3][CF_3SO_3]_3$, at 30 K (CSD 1879270). We found the low temperature structure to be virtually identical to the 120 K one (CSD 1879267, Table S1), but due to the sensitivity of the electronic structure, CASSCF-SO-calculated EPR spectra show non-negligible changes (Figure 9). It is interesting to note that the X-band EPR trace calculated using the 30 K structure agrees better with the experimental data, however, the broad feature (0.2 – 0.4 T at X-band) is not accounted for by either of these structures and is better accounted for with the distribution model for B_2^0 discussed above.

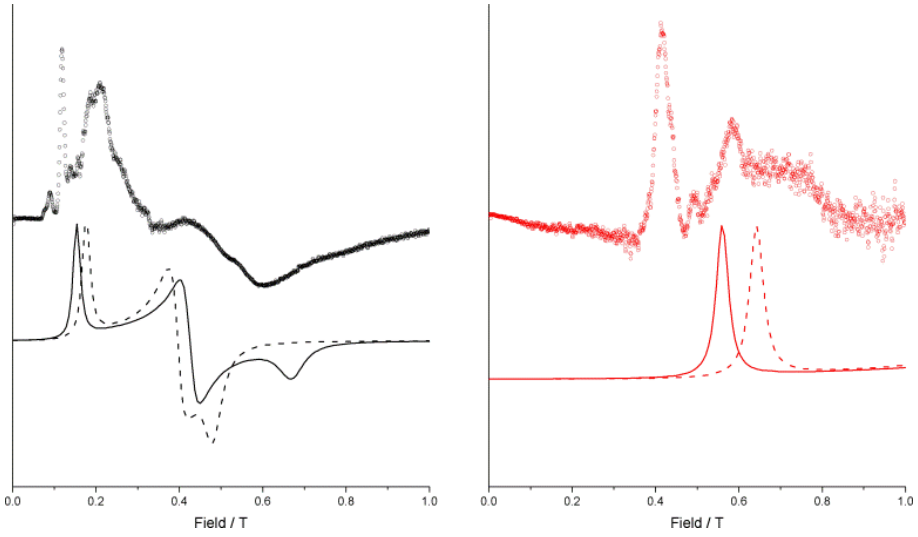

Figure 9. EPR simulations for $[YbL^3][CF_3SO_3]_3$. Experimental data (open circles) at X-band (black) and Q-band (red), compared to CASSCF-SO simulated EPR traces based on XRD structures at 120 K (dashed lines) and 30 K (solid lines). EPR spectra collected at 5 K, and simulated using an isotropic 1 (X-band) or 2 GHz (Q-band) linewidth.

(iv) Solvent disorder

In both the $[LnL^2]$ and $[LnL^3][CF_3SO_3]_3$ samples there are disordered solvent molecules in the lattice. For $[LnL^3][CF_3SO_3]_3$ a methanol molecule sits above the oxygen donor pocket on the C_3 axis with a disordered methyl group over three symmetry-related positions, whereas in $[LnL^2]$ there are highly disordered water and methanol molecules. Interestingly, for $[LnL^3][CF_3SO_3]_3$ the occupancy of the methanol molecule is less than one, and in the reported structures it has been fixed to a value of 0.5, meaning that inside the same crystal some $[LnL^3][CF_3SO_3]_3$ units have a proximate non-coordinated solvent molecule and some do not. Notably for $[YbL^3][CF_3SO_3]_3$, an isomorphous phase with the same unit cell parameters but lacking the methanol molecule has been previously reported (CSD 965911). To examine the impact of this on the EPR spectra, we have performed CASSCF-SO calculations for $[LnL^3][CF_3SO_3]_3$ with and without the methanol molecule, finding significant changes in the electronic structure between the two cases (Tables S18-S19 and Figures S31-S32), despite the methanol molecule not being directly coordinated to the Ln^{III} ion. The presence of the methanol molecule breaks the axial symmetry of $[YbL^3][CF_3SO_3]_3$: this has little impact on magnetic data but has huge effects on the EPR traces. Calculated EPR spectra for the two different environments of $[YbL^3][CF_3SO_3]_3$ show that the ground doublet changes from easy-plane to easy-axis, following addition of the non-coordinating methanol molecule (Figure 10). The change in the ground state is highlighted by a change in sign of B_2^0 which is positive without MeOH and negative with MeOH (Table

S18). The presence of different low-field resonances (Figure 10, *ca.* 0.20 and 0.4 T at X-band) for the two coordination environments, suggest that the two experimental features in this region could arise from the solvated and non-solvated molecules in the same sample. It is intriguing that a similar EPR trace with a narrow and a broad signal at lower field is found for [YbL^2] in which, similarly to [YbL^3][CF_3SO_3]$_3$, there is solvent disorder (Figure 5). For [YbL^1], which has well-defined crystallographic solvation, the EPR trace does not show any broad feature and is well-modelled with the S = 1/2 approach (Figure 5). These results are in line with a rich literature of examples where the impact of the first and second coordination sphere as well as crystal packing and counterions on the magnetic anisotropy and electronic structure of metal complexes have been studied, both experimentally and theoretically.[23,29–33]

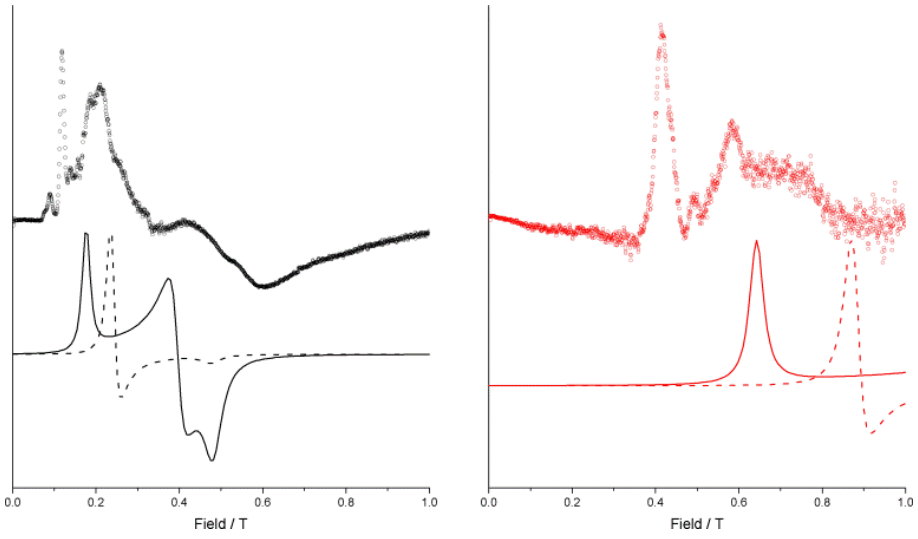

Figure 10. EPR simulations for [YbL^3][CF_3SO_3]$_3$. EPR traces at X-band (black) and Q-band (red), experimental data (open circles) and simulated EPR traces based on CASSCF-SO calculations of structures at 120 K in which an axial non-coordinating molecule of methanol is included (solid line) or omitted (dashed line).

Conclusions

We have presented the magnetic data and EPR spectra for a series of nine-coordinate (pseudo-)C_3 lanthanide complexes in the solid state. Single-point CASSCF-SO calculations based on the known or surrogate crystal structures do not consistently describe the experimental data. Moreover, 5 K EPR spectra for [LnL$^{1\text{-}3}$] (Ln = Dy, Er, Yb) can be interpreted with an S = 1/2 model only in a limited number of examples. Based on our experience from solution studies of [LnL^1], where near-zero values of B_2^0 mean that small distortions in the coordination environment can drastically change the magnetic anisotropy, we suggest that such hypersensitivity likely persists in the solid state for [LnL$^{1\text{-}3}$] and thus knowledge of the crystal structure is insufficient to interpret the experimental data. The solid-state magnetic and spectroscopic properties likely depend on a number of factors that are impossible to disentangle: a distribution of structural parameters generates a distribution of B_2^0 values; the electronic structure is sensitive to thermal variations of the crystal structure; there are thermally accessible EPR-active excited states; disorder in non-coordinated solvent molecules impacts the local electronic structure. All of these effects are likely to be present to differing degrees across [LnL$^{1\text{-}3}$], and hence great care should be taken in the interpretation of EPR spectra for systems with small magnetic anisotropy, even when the molecular structure is "known" from XRD.

Supporting Information. Crystallographic data, CASSCF-SO calculations details, Calculated EPR spectra, TGA, and elemental analysis.

Corresponding Authors

Nicholas F. Chilton, Email: nicholas.chilton@manchester.ac.uk

David Parker, Email: david.parker@durham.ac.uk

Funding Sources

We thank the EPSRC (EP/N007034/1 and EP/N006909/1), The University of Manchester, Durham University, and the Ramsay Memorial Trust for funding.

Acknowledgment

We thank the EPSRC National EPR Facility for access to the SQUID magnetometer and EPR spectrometers. We thank Prof. Ilya Kuprov and Dr Elizaveta Suturina (Southampton) for useful discussions.

References

(1) Piguet, C.; Geraldes, C. F. G. C. Paramagnetic NMR Lanthanide Induced Shifts for Extracting Solution Structures. In *Handbook on the Physics and Chemistry of Rare Earths, Volume 33*; 2003; pp 353–463.

(2) Faulkner, S.; Blackburn, O. A. The Chemistry of Lanthanide MRI Contrast Agents. In *The Chemistry of Molecular Imaging*; Long, N., Wong, W.-T., Eds.; John Wiley & Sons, Inc: Hoboken, NJ, 2014; pp 179–197.

(3) Goodwin, C. A. P.; Ortu, F.; Reta, D.; Chilton, N. F.; Mills, D. P. Molecular Magnetic Hysteresis at 60 Kelvin in Dysprosocenium. *Nature* **2017**, *548* (7668), 439–442.

(4) Sessoli, R. Materials Science: Magnetic Molecules Back in the Race. *Nature* **2017**, *548* (7668), 400–401.

(5) Parker, D. Rare Earth Coordination Chemistry in Action. In *Handbook on the Physics and Chemistry of Rare Earths, Volume 50*; 2016; pp 269–299.

(6) Finney, K.-L. N. A.; Harnden, A. C.; Rogers, N. J.; Senanayake, P. K.; Blamire, A. M.; O'Hogain, D.; Parker, D. Simultaneous Triple Imaging with Two PARASHIFT Probes: Encoding Anatomical, PH and Temperature Information Using Magnetic Resonance Shift Imaging. *Chem. - A Eur. J.* **2017**, *23* (33), 7976–7989.

(7) Bleaney, B. Nuclear Magnetic Resonance Shifts in Solution Due to Lanthanide Ions. *J. Magn. Reson.* **1972**, *8* (1), 91–100.

(8) Bleaney, B.; Dobson, C. M.; Levine, B. A.; Martin, R. B.; Williams, R. J. P.; Xavier, A. V. Origin of Lanthanide Nuclear Magnetic Resonance Shifts and Their Uses. *J. Chem. Soc. Chem. Commun.* **1972**, No. 13, 791–793.

(9) Vonci, M.; Mason, K.; Suturina, E. A.; Frawley, A. T.; Worswick, S. G.; Kuprov, I.; Parker, D.; McInnes, E. J. L.; Chilton, N. F. Rationalisation of Anomalous Pseudo-Contact Shifts and Their Solvent Dependence in a Series of C 3 -Symmetric Lanthanide Complexes. *J. Am. Chem. Soc.* **2017**, jacs.7b07094.

(10) Funk, A. M.; Finney, K. L. N. A.; Harvey, P.; Kenwright, A. M.; Neil, E. R.; Rogers, N. J.; Kanthi Senanayake, P.; Parker, D. Critical Analysis of the Limitations of Bleaney's Theory of Magnetic Anisotropy in Paramagnetic Lanthanide Coordination Complexes. *Chem. Sci.* **2015**, *6* (3), 1655–1662.

(11) Rinehart, J. D.; Long, J. R. Exploiting Single-Ion Anisotropy in the Design of f-Element Single-Molecule Magnets. *Chem. Sci.* **2011**, *2* (11), 2078–2085.

(12) Chilton, N. F.; Collison, D.; McInnes, E. J. L.; Winpenny, R. E. P.; Soncini, A. An Electrostatic Model for the Determination of Magnetic Anisotropy in Dysprosium

Complexes. *Nat. Commun.* **2013**, *4*, 2551.

(13) Gateau, C.; Mazzanti, M.; Pécaut, J.; Dunand, F. A.; Helm, L. Solid-State and Solution Properties of the Lanthanide Complexes of a New Nonadentate Tripodal Ligand Derived from 1,4,7-Triazacyclononane. *Dalt. Trans.* **2003**, No. 12, 2428–2433.

(14) Nocton, G.; Nonat, A.; Gateau, C.; Mazzanti, M. Water Stability and Luminescence of Lanthanide Complexes of Tripodal Ligands Derived from 1,4,7-Triazacyclononane: Pyridinecarboxamide versus Pyridinecarboxylate Donors. *Helv. Chim. Acta* **2009**, *92* (11), 2257–2273.

(15) Walton, J. W.; Bari, L. Di; Parker, D.; Pescitelli, G.; Puschmann, H.; Yufit, D. S. Structure, Resolution and Chiroptical Analysis of Stable Lanthanide Complexes of a Pyridylphenylphosphinate Triazacyclononane Ligand. *Chem. Commun.* **2011**, *47* (45), 12289.

(16) Walton, J. W.; Carr, R.; Evans, N. H.; Funk, A. M.; Kenwright, A. M.; Parker, D.; Yufit, D. S.; Botta, M.; De Pinto, S.; Wong, K.-L.; et al. Isostructural Series of Nine-Coordinate Chiral Lanthanide Complexes Based on Triazacyclononane. *Inorg. Chem.* **2012**, *51* (15), 8042–8056.

(17) Neil, E. R.; Funk, A. M.; Yufit, D. S.; Parker, D. Synthesis, Stereocontrol and Structural Studies of Highly Luminescent Chiral Tris-Amidepyridyl-Triazacyclononane Lanthanide Complexes. *Dalt. Trans.* **2014**, *43* (14), 5490–5504.

(18) Dolomanov, O. V.; Bourhis, L. J.; Gildea, R. J.; Howard, J. A. K.; Puschmann, H. OLEX2 : A Complete Structure Solution, Refinement and Analysis Program. *J. Appl.*

Crystallogr. **2009**, *42* (2), 339–341.

(19) Sheldrick, G. M. SHELXT – Integrated Space-Group and Crystal-Structure Determination. *Acta Crystallogr. Sect. A Found. Adv.* **2015**, *71* (1), 3–8.

(20) Sheldrick, G. M. Crystal Structure Refinement with SHELXL. *Acta Crystallogr. Sect. C Struct. Chem.* **2015**, *71* (1), 3–8.

(21) Aquilante, F.; Autschbach, J.; Carlson, R. K.; Chibotaru, L. F.; Delcey, M. G.; De Vico, L.; Fdez. Galván, I.; Ferré, N.; Frutos, L. M.; Gagliardi, L.; et al. <scp>Molcas</Scp> 8: New Capabilities for Multiconfigurational Quantum Chemical Calculations across the Periodic Table. *J. Comput. Chem.* **2016**, *37* (5), 506–541.

(22) Chibotaru, L. F.; Ungur, L. Ab Initio Calculation of Anisotropic Magnetic Properties of Complexes. I. Unique Definition of Pseudospin Hamiltonians and Their Derivation. *J. Chem. Phys.* **2012**, *137* (6), 064112.

(23) Pedersen, K. S.; Ungur, L.; Sigrist, M.; Sundt, A.; Schau-Magnussen, M.; Vieru, V.; Mutka, H.; Rols, S.; Weihe, H.; Waldmann, O.; et al. Modifying the Properties of 4f Single-Ion Magnets by Peripheral Ligand Functionalisation. *Chem. Sci.* **2014**, *5* (4), 1650.

(24) Roos, B. O.; Lindh, R.; Malmqvist, P.-Å.; Veryazov, V.; Widmark, P.-O. New Relativistic ANO Basis Sets for Transition Metal Atoms. *J. Phys. Chem. A* **2005**, *109* (29), 6575–6579.

(25) Ungur, L.; Chibotaru, L. F. Ab Initio Crystal Field for Lanthanides. *Chem. - A Eur. J.* **2017**, *23* (15), 3708–3718.

(26) Chilton, N. F.; Anderson, R. P.; Turner, L. D.; Soncini, A.; Murray, K. S. PHI: A Powerful New Program for the Analysis of Anisotropic Monomeric and Exchange-Coupled Polynuclear d - and f -Block Complexes. *J. Comput. Chem.* **2013**, *34* (13), 1164–1175.

(27) Mason, K.; Harnden, A. C.; Patrick, C. W.; Poh, A. W. J.; Batsanov, A. S.; Suturina, E. A.; Vonci, M.; McInnes, E. J. L.; Chilton, N. F.; Parker, D. Exquisite Sensitivity of the Ligand Field to Solvation and Donor Polarisability in Coordinatively Saturated Lanthanide Complexes. *Chem. Commun.* **2018**, *54* (61), 8486–8489.

(28) Husein Mor, H.; Weihe, H.; Bendix, J. Fitting of EPR Spectra: The Importance of a Flexible Bandwidth. *J. Magn. Reson.* **2010**, *207* (2), 283–286.

(29) Canaj, A. B.; Singh, M. K.; Wilson, C.; Rajaraman, G.; Murrie, M. Chemical and in Silico Tuning of the Magnetisation Reversal Barrier in Pentagonal Bipyramidal Dy(Iii) Single-Ion Magnets. *Chem. Commun.* **2018**, *54* (59), 8273–8276.

(30) Sottini, S.; Poneti, G.; Ciattini, S.; Levesanos, N.; Ferentinos, E.; Krzystek, J.; Sorace, L.; Kyritsis, P. Magnetic Anisotropy of Tetrahedral Co II Single-Ion Magnets: Solid-State Effects. *Inorg. Chem.* **2016**, *55* (19), 9537–9548.

(31) Vonci, M.; Giansiracusa, M. J.; Gable, R. W.; Van den Heuvel, W.; Latham, K.; Moubaraki, B.; Murray, K. S.; Yu, D.; Mole, R. A.; Soncini, A.; et al. Ab Initio Calculations as a Quantitative Tool in the Inelastic Neutron Scattering Study of a Single-Molecule Magnet Analogue. *Chem. Commun.* **2016**, *52* (10), 2091–2094.

(32) Rigamonti, L.; Nava, A.; Boulon, M.-E.; Luzon, J.; Sessoli, R.; Cornia, A. Experimental

and Theoretical Studies on the Magnetic Anisotropy in Lanthanide(III)-Centered Fe 3 Ln Propellers. *Chem. - A Eur. J.* **2015**, *21* (34), 12171–12180.

(33) Cucinotta, G.; Perfetti, M.; Luzon, J.; Etienne, M.; Car, P.-E.; Caneschi, A.; Calvez, G.; Bernot, K.; Sessoli, R. Magnetic Anisotropy in a Dysprosium/DOTA Single-Molecule Magnet: Beyond Simple Magneto-Structural Correlations. *Angew. Chemie Int. Ed.* **2012**, *124* (7), 1638–1642.

(34) Denning, R. G.; Harmer, J.; Green, J. C.; Irwin, M. Covalency in the 4f Shell of Tris - Cyclopentadienyl Ytterbium ($YbCp_3$) — A Spectroscopic Evaluation. *J. Am. Chem. Soc.* **2011**, 133 (50), 20644–20660.

TOC:

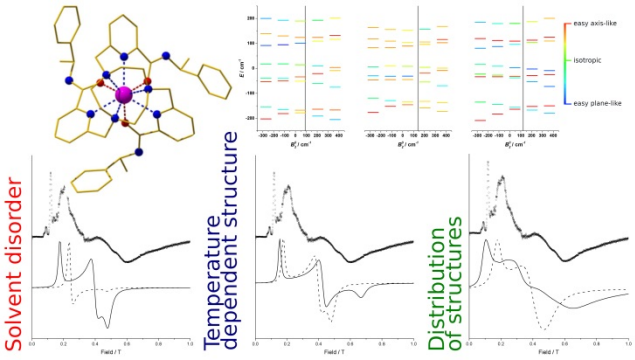

Knowing the crystal structure is often sufficient to interpret the properties of small molecules. We show that a series lanthanide complexes have geometrically hypersensitive electronic structures, rendering the magnetic and spectroscopic properties very difficult to interpret. We explore possible explanations for peculiar electron paramagnetic resonance spectra and conclude that a number of entangled factors are at play, including a distribution of structural parameters, thermal variations of the crystal structure, electronic excited states, and disorder in non-coordinated solvent molecules.